https://doi.org/10.5194/egusphere-2026-4938
Preprint. Discussion started: 27 August 2026

Structural divergence between satellite and surface CO observations across China, North America, and Europe (2015–2024)

Zhaojun Tang[1], Zhe Jiang[1]*, Panpan Yang[1], Jiaqi Chen[2], Pingqing Fu[1] and Yanan Shen[3]

[1]Institute of Surface–Earth System Science, School of Earth System Sciences, Tianjin University, Tianjin, 300072, China.
[2]Anhui Institute of Meteorological Sciences, Hefei, Anhui, 230031, China.
[3]School of Earth and Space Sciences, University of Science and Technology of China, Hefei, Anhui, 230026, China.

*Correspondence to: Zhe Jiang (zhejiang@tju.edu.cn)

Abstract

Satellite and surface observations of atmospheric carbon monoxide (CO) yield divergent emission estimates, yet the underlying causes of this discrepancy remain poorly understood. Here we present a multi-region analysis spanning 2015-2024 over China, North America, and Europe, assimilating MOPITT satellite retrievals and ground-based CO measurements from over 3300 monitoring stations. Our results reveal that the systematic underestimation of modeled surface CO is a common feature across all three continents, with median observation-to-model ratios of 1.82 (China), 1.65 (North America), and 2.25 (Europe). This bias progressively diminishes from urban to rural sites, by 44% in North America and 58% in Europe, and almost disappears at remote sites, demonstrating that representation error is an important driver of the surface-model mismatch. In contrast, comparisons of column CO between MOPITT and model show no systematic underestimation. Assimilation experiments further illuminate the structural nature of this divergence: while surface-data assimilation greatly improves agreement with in situ observations, it introduces a positive column bias relative to MOPITT. This bias is most pronounced over China and Europe but remains modest over North America, and accordingly the decadal trends from surface CO show a sharp decline in China (-5.92% yr^{-1}) vs. plateaus after 2018 and 2016 in North America and Europe, while

https://doi.org/10.5194/egusphere-2026-4938
Preprint. Discussion started: 27 August 2026

satellite-derived column trends are substantially weaker. Our multi-region analysis demonstrates that the satellite-surface discrepancy is a structurally embedded feature of the observing system, and advocates for joint utilization of both observation platforms in future inversion studies to achieve robust and self-consistent CO emission estimates.

1. Introduction

Atmospheric carbon monoxide (CO) is a key trace gas affecting tropospheric chemistry and air quality, with major sources including fossil fuel combustion, biomass burning, and hydrocarbon oxidation. Through its role as a major sink of hydroxyl radicals (OH) and a precursor to tropospheric ozone, CO exerts significant influence on the atmosphere's oxidizing capacity and secondary pollutant formation. Satellite observations, with global coverage, have been widely used to investigate atmospheric CO changes (Han et al., 2018; Jeffery et al., 2024) and constrain CO emissions (Zheng et al., 2019; Fortems-Cheiney et al., 2024; Tang et al., 2026). Meanwhile, surface measurements from ground-based monitoring networks provide high temporal resolution and direct measurements of CO concentrations at the surface level, enabling detailed assessments of local emission changes and air quality impacts (Zhou et al., 2017; Feng et al., 2020b; Xie et al., 2025). Recent advances in computational techniques further enabled the integration of satellite and surface CO observations with machine learning models (Han et al., 2022; Wei et al., 2023), thereby deepening our understanding of CO sources and spatiotemporal variations.

However, a growing body of inverse modeling studies reveals a notable discrepancy between CO emission estimates derived from satellite and surface observations. Emission estimates based on satellite data generally find limited adjustments relative to a priori inventories: for instance, Zheng et al. (2019) and Fortems-Cheiney et al. (2024) reported a posteriori CO emission estimates in China and Europe about 1-5% lower than the respective a

https://doi.org/10.5194/egusphere-2026-4938
Preprint. Discussion started: 27 August 2026

priori estimates, while Tang et al. (2026) suggested a upward adjustment of 5-9% for China. By contrast, inversions using surface observations indicate much larger underestimations, for example, Feng et al. (2020a) and Jia et al. (2025) reported that CO emissions in China could be underestimated by 180-250%. This divergence points to a potential systematic discrepancy between satellite and surface CO observations, particularly over China, underscoring the need for a thorough understanding of the drivers of this discrepancy to ensure accurate use and interpretation of CO datasets.

Understanding this discrepancy requires recognizing the inherent limitations of each observation type. Limited vertical resolution of satellite measurements means that retrieved lower-tropospheric CO signals are inevitably mixed with contributions from the free troposphere (Jiang et al., 2013; Tang et al., 2024), and thus satellite-derived CO fields are more susceptible to influences from long-range transport, making it difficult to isolate local source signals. On the other hand, surface CO measurements suffer from representation errors when compared to grid-based model simulations. Monitoring stations, particularly in urban areas, sample air masses that may not be representative of the model grid average (Fang et al., 2024; Fang et al., 2026), and uncertainties in planetary boundary layer mixing further complicate the interpretation (Castellanos et al., 2011; Du et al., 2020). These complementary strengths and weaknesses imply that the discrepancies between their respective inversion results of CO emissions may reflect fundamental differences in what each measurement actually represents. As a preliminary attempt to explore this issue, Tang et al. (2022) compared assimilated CO fields from MOPITT and surface measurements over China (2015-2020) and found that surface observations showed persistently higher concentrations and a steeper declining trend than those inferred from satellite data.

In this study, we move beyond single-region analyses by constructing a unified multi-region assimilation framework spanning China, North America, and Europe for the period

https://doi.org/10.5194/egusphere-2026-4938
Preprint. Discussion started: 27 August 2026

2015-2024, assimilating both MOPITT satellite retrievals and ground-based CO measurements from over 3300 stations. This design directly tests a central hypothesis: whether the satellite-surface discrepancy is a region-specific artifact tied to Chinese emissions and monitoring networks, or instead reflects a fundamental structural difference between the two observation platforms. A key methodological innovation is the systematic stratification of surface sites into urban, suburban, rural, and remote categories, enabled by independent mapping rules for each monitoring network, which allows us to quantitatively disentangle the contribution of representation error from systematic biases in emission inventories. Through this lens, we pursue three interconnected objectives: (1) to diagnose the magnitude and spatial structure of the model-observation mismatch in surface CO across continents, and to attribute its drivers via the urban-to-rural gradient; (2) to conduct cross-validation assimilation experiments that test how surface-data assimilation improves in situ agreement while potentially altering column CO consistency with MOPITT; and (3) to assess decadal trends (2015-2024) in CO concentrations, evaluating how the choice of observation platforms shapes the inferred rate of CO change and its sensitivity to background transport vs. local emissions. By integrating these lines of evidence, this study aims to deliver a robust diagnostic for reconciling multi-platform CO observations, offering actionable guidance for future inversion systems that seek to harness the strengths of both satellite and surface measurements while mitigating their respective limitations.

The paper is organized as follows: Section 2 describes the multi-platform observations (MOPITT satellite retrievals and ground-based measurements from three continents), the GEOS-Chem model configuration, and the suboptimal Kalman filter assimilation method. Section 3 presents the comparative results and discussion, focusing on the systematic underestimation of modeled surface CO and the role of representation error, the contrasting impacts of satellite vs. surface data assimilations, and the decadal trends in CO concentrations.

https://doi.org/10.5194/egusphere-2026-4938
Preprint. Discussion started: 27 August 2026

Conclusions are given in Section 4.

2. Data and Methodology

2.1 MOPITT CO Retrievals

The MOPITT was launched aboard the NASA Terra spacecraft on December 18, 1999. Terra operates in a sun-synchronous polar orbit at an altitude of approximately 705 km and crosses the equator at about 10:30 local time. MOPITT has a cross-track scan width of approximately 612 km, with an individual pixel footprint of about 22 km × 22 km. The MOPITT CO data used in this study are from the version 9J joint retrieval product. This product retrieves vertical CO profiles using an optimal estimation approach that combines radiance information from the thermal infrared channel (TIR; 4.7 μm) and the near-infrared channel (NIR; 2.3 μm) (Worden et al., 2010; Deeter et al., 2022). The retrieved CO volume mixing ratios are reported as layer averages at 10 pressure levels, including the surface, 900, 800, 700, 600, 500, 400, 300, 200, and 100 hPa. The relationship between the retrieved CO profile and the true atmospheric state can be expressed as $\boldsymbol{z}_{\mathrm{ret}} = \boldsymbol{z}_a + \mathbf{A}(\boldsymbol{z} - \boldsymbol{z}_a) + \boldsymbol{G}_\epsilon$, where $\boldsymbol{z}_{\mathrm{ret}}$ is the retrieved CO profile, $\boldsymbol{z}_a$ is the MOPITT a priori profile, $\boldsymbol{z}$ is the true atmospheric state, $\mathbf{A}$ is the averaging kernel matrix, which characterizes the sensitivity of the retrieval to the true vertical distribution of CO, and $\boldsymbol{G}_\epsilon$ represents the retrieval error term. In the data screening procedure, we only retained cloud-free observations with Cloud Description = 2. Since the NIR channel relies on reflected solar radiation, nighttime observations were not included in the analysis.

2.2 Ground-Based Air Quality Observations

This study used hourly ground-based CO concentration observations from China, North America, and Europe. The data were obtained from the China Ministry of Ecology and Environment (MEE) national air quality monitoring network, the United States (US)

https://doi.org/10.5194/egusphere-2026-4938
Preprint. Discussion started: 27 August 2026

Environmental Protection Agency (EPA) Air Quality System (AQS), the Canadian National Air Pollution Surveillance (NAPS) program, and the European Environment Agency (EEA) air quality monitoring database. To ensure cross-regional comparability, all CO concentration data units were converted to ppb. Specifically, US and Canadian data in ppm were multiplied by 1000 to convert to ppb, while mg m^{-3} unit data from China and Europe were converted based on the ideal gas law. Considering that reference temperature for observations in China changed from 273 K to 298 K on September 1, 2018, observations from that date onward were converted back to 273 K reference state to ensure consistency in the 2015-2024 time series.

After unit conversion, abnormal observations with values ≤0 or >6000 ppb were removed and treated as missing. On this basis, two annual quality control checks were applied at the site-year level. A given year was flagged as an unqualified year if the fraction of valid observation days was below 75% or if the maximum consecutive missing-data gap within that year was ≥10 days. To ensure the representation and temporal stability of sites for the long-term analysis over 2015-2024, an additional cross-year consistency check was performed at the site level. A site was included in the long-term analysis only if at least 80% of its 10 years were qualified years, and the full 10-year observation record was retained for such sites. After quality control, the site observations were spatiotemporally paired with the corresponding GEOS-Chem grids. Finally, 1931 long-term stable sites in China, 430 in North America, and 984 in Europe were retained. To characterize the spatial representation of ground monitoring sites for CO concentrations, this study assigned a representation scale parameter L in kilometers to each site based on the native metadata fields of each monitoring network. This parameter represents the approximate spatial range over which the observation is considered representative. Due to differences in the classification systems adopted by various monitoring networks, independent mapping rules were specifically constructed based on study in Elbern et al. (2007) (see details in Table S1).

https://doi.org/10.5194/egusphere-2026-4938
Preprint. Discussion started: 27 August 2026

2.3 GEOS-Chem Model

This study used the GEOS-Chem (v14.6.2) three-dimensional global atmospheric chemistry transport model to simulate CO concentrations. The model is driven by MERRA-2 reanalysis meteorological data. The global default anthropogenic emissions were taken from the Community Emissions Data System for CMIP6 (CEDS-CMIP6) inventory (Hoesly et al., 2018). For Asia, these emissions were replaced by MIX v2 (Li et al., 2024). Over the US, anthropogenic emissions were taken from the 2016 National Emissions Inventory (NEI2016), while over Europe the global CEDS-CMIP6 inventory was retained. Biomass burning emissions were obtained from the Global Fire Emissions Database version 5 (GFED5) (van der Werf et al., 2025). Biogenic volatile organic compound (BVOC) emissions were calculated using the Model of Emissions of Gases and Aerosols from Nature version 2.1 (MEGAN v2.1) (Guenther et al., 2006). The simulations were conducted using a nested-domain configuration with a horizontal resolution of 0.5° × 0.625°. A CO-only simulation was performed, in which the chemistry, emissions, transport, and deposition processes of CO were calculated. The chemical loss of CO is primarily controlled by oxidation by OH, and the OH fields used here were obtained from archived monthly mean concentrations from a full-chemistry GEOS-Chem simulation. The lateral boundary conditions for the nested domain were provided by a 4° × 5° global GEOS-Chem simulation and updated every 3 h to represent the influence of transport from outside the regional domain on CO concentrations within the simulation region.

2.4 Kalman Filter Assimilation Method

This study assimilated MOPITT and ground-based CO observations using the suboptimal Kalman filter method to optimize CO concentration fields, as described by Tang et al. (2022). Briefly, the model first advances the analysis field from the previous time step to obtain the background field, $\boldsymbol{x}_t^b = \mathbf{M}(\boldsymbol{x}_{t-1}^a)$, and then corrects the CO concentration through the Kalman update, $\boldsymbol{x}_t^a = \boldsymbol{x}_t^b + \mathbf{G}_t(\boldsymbol{y}_t - \mathbf{K}_t\boldsymbol{x}_t^b)$, where $\boldsymbol{y}_t$ is the observation vector, $\mathbf{K}_t$ is the

https://doi.org/10.5194/egusphere-2026-4938
Preprint. Discussion started: 27 August 2026

observation operator, and $\mathbf{G}_t$ is the Kalman gain. The Kalman gain is defined as $\mathbf{G}_t = \mathbf{S}_t^b \mathbf{K}_t^{\mathrm{T}} (\mathbf{K}_t \mathbf{S}_t^b \mathbf{K}_t^{\mathrm{T}} + \mathbf{S}_\epsilon)^{-1}$, where $\mathbf{S}_t^b$ and $\mathbf{S}_\epsilon$ are the model background error covariance and observation error covariance, respectively.

The assimilation experiment started on July 1, 2014, to generate optimized initial conditions for January 1, 2015. Thereafter, a 1 h assimilation window was used to update the model CO concentration field hourly and advance it to the next time step. The MOPITT observation error was determined from the error covariance matrix provided in the product. The ground-based observation error included both measurement error and representation error. The measurement error was calculated as $\epsilon_0 = \epsilon_{\max} + 0.0075\Pi_0$, where $\epsilon_{\max} = 6$ ppb and Π_0 is the observed CO concentration. The representation error was calculated as $\epsilon_r = \gamma\epsilon_0\sqrt{\Delta l / L}$, where $\gamma = 0.5$, Δl is the model horizontal resolution, and L is the site representation scale (see details in Table S1). The total ground-based observation error was defined as $\epsilon = \sqrt{\epsilon_0^2 + \epsilon_r^2}$. To reduce single-site representation errors, multiple ground-based observations within the same model grid cell were combined into grid-scale observations using the super-observation approach (Miyazaki et al., 2017; Feng et al., 2020b).

3. Results and Discussions

3.1 Discrepancy between modeled and observed CO concentrations

3.1.1 Systematic underestimation in modeled surface CO

We first diagnose the magnitude and spatial structure of the model-observation mismatch in surface CO concentrations across the three continents. As a starting point, we evaluate the spatial distribution of CO concentrations from the GEOS-Chem a priori simulations (Figs. 1a-c). The model successfully reproduces large-scale spatial gradients of CO concentrations, revealing contrasts in emission intensity across the three continents. In China (Fig. 1a), the a priori CO field exhibits a pronounced pollution dome, with peak concentrations exceeding 400

https://doi.org/10.5194/egusphere-2026-4938
Preprint. Discussion started: 27 August 2026

ppb concentrated over the North China Plain (NCP), Yangtze River Delta (YRD), and Sichuan Basin (SCB). In contrast, North America (Fig. 1b) shows a more subdued pollution pattern. Localized enhancements occur along the West Coast and in the Northeastern megalopolises, where modeled CO concentrations can reach 200 ppb. Europe (Fig. 1c) presents a complex, multi-center distribution driven by its dense network of urban and industrial centers. The highest a priori CO concentrations, exceeding 150 ppb, are found over the Po Valley, Benelux region, and parts of Central Europe.

Despite these seemingly reasonable large-scale patterns, a dramatic discrepancy emerges when the a priori CO fields are evaluated against surface observations (Figs. 1d-f). The median of observation-to-model (Obs/Mod) ratios reaches 1.82 (mean: 2.08) in China (Fig. 2a), consistent with the suggested underestimation of CO emissions by approximate 180-250% (Feng et al., 2020b; Jia et al., 2025). Particularly high ratios (>4.0) appear in western, northeastern, and some background stations (Fig. 1d). This spatial pattern of bias is further quantified in the scatter relationship between simulations and observations (Figs. 3a-d), which shows a correlation coefficient (R) of 0.31, a regression slope (k) of 0.22 and mean bias of -331.4 ppb over the entire China domain (Table 1.1); as well as 0.47 (R), 0.24 (k) and -399.8 ppb (bias) in the NCP; 0.28 (R), 0.43 (k) and -139.6 ppb (bias) in the YRD; and 0.43 (R), 0.28 (k) and -257.8 ppb (bias) in the SCB (Table S2.1), respectively.

Moving to North America, the median Obs/Mod ratio is 1.65 (mean: 1.92), lower than that in China (Fig. 2b). Extreme underestimation is rare, with only six sites showing ratios >5.0. Moderate underestimation (ratios ~2–4) prevails across most of the continent, with slightly elevated ratios along the West Coast and in some urbanized areas. Over the entire North American domain, the R is 0.23, the k is 0.07, and the mean bias is -198.9 ppb (Table 1.1). A similar yet more severe pattern of underestimation characterizes Europe. The Obs/Mod ratio (Fig. 2c) is the highest among the three continents: the median is 2.25 (mean: 2.52), with 57

https://doi.org/10.5194/egusphere-2026-4938
Preprint. Discussion started: 27 August 2026

sites (~5.7%) having ratios above 5.0, predominantly located in the Apennine Peninsula. The consistency for Europe is the lowest among the three regions, with R = 0.29, k = 0.03, and a mean bias of -244.7 ppb (Table 1.1). While China exhibits the largest absolute negative mean bias (-331.4 ppb) due to its higher ambient CO concentrations, it also demonstrates the largest slope (k = 0.22). This is significantly larger than the slopes observed in North America (k = 0.07) and Europe (k = 0.03).

3.1.2 Role of site representation error: stratification by station type

To further investigate the underlying causes of model underestimation, we stratified surface sites by type, i.e., urban, suburban, rural, and remote, across the three continents. This classification allows us to assess how representation error, arising from the coarse resolution of the model relative to local emission gradients, contributes to the systematic bias. Notably, China's monitoring network includes only urban and suburban station types, whereas North America and Europe offer a more complete spectrum of site classifications (urban, suburban, rural, and remote). This contrast motivates our extension of the analysis to the latter two continents, enabling a more comprehensive evaluation of the role of site representativeness. In China, both urban and suburban sites exhibit nearly twofold underestimation (Table 2): the median and mean ratios are 1.80 and 2.05 for urban sites, and 1.96 and 2.27 for suburban sites, respectively.

By contrast, a clear gradient emerges in North America with median ratios of 1.77, 1.64, 1.43, and 1.21 across urban, suburban, rural, and remote sites, respectively (Table 2), which means that from urban sites to rural sites, the model's negative bias was reduced by 44%; while from urban sites to remote sites, the model's negative bias was reduced by 73%. Similarly, the median ratios are 2.30, 2.17, 1.55, and 0.94 across urban, suburban, rural, and remote sites in Europe, respectively (Table 2), which means that from urban sites to rural sites, the model's negative bias was reduced by 58% (comparable to that of North America); while the model's

https://doi.org/10.5194/egusphere-2026-4938
Preprint. Discussion started: 27 August 2026

negative bias completely disappeared at remote sites (due to the limited number of sites, the reliability of the analysis at remote sites is limited in Europe). Since this site type sequence typically corresponds to decreasing influence from local anthropogenic emissions, this result suggests that model-observation discrepancies in surface CO concentrations may diminish as local emission impacts weaken. It is consistent with the smoothing effect of coarse-resolution, implying that representation error is an important source of underestimation in model surface CO concentrations.

3.1.3 Evidence from model-observation discrepancy in column CO

We have suggested that the model-observation discrepancy in surface CO concentrations could be partially attributed to representation error, here we further compare the modeled CO column concentrations against satellite retrievals to provide an independent, large-scale evaluation. Figs. 1g-i show the ratios between MOPITT and modeled CO column concentrations (MOP/Mod) across three continents. In China, the ratios of MOP/Mod are greater than 1 in the NCP and Northeast China, reaching approximately 1.2-1.4 in some areas, while being less than 1 in other regions. In North America, the ratios are greater than 1 in northern regions. In Europe, the ratios are greater than 1 in the eastern and northern regions. Overall, the R is 0.73, the k is 0.62, and the mean bias is 6.8 ppb in China (Table 1.2), as well as 0.30 (R), 0.14 (k) and 3.1 ppb (bias) in North America; and 0.22 (R), 0.08 (k) and 1.8 ppb (bias) in Europe. Similar to surface CO concentrations, the modeled CO column concentrations show larger R and slope when compared with satellite observations over China than those over North America and Europe.

Comparing the findings of Section 3.1.2 with those of this section yields a coherent picture. Ground-based observations indicate that modeled surface CO is strongly biased low (-198.9 to -331.4 ppb across three continents, Table 1.1). In contrast, the column CO comparison reveals no systematic underestimation; instead, biases are slightly positive (1.8-6.8 ppb across

https://doi.org/10.5194/egusphere-2026-4938
Preprint. Discussion started: 27 August 2026

three continents, Table 1.2). Because column CO integrates the entire atmosphere, it is less sensitive to local emission gradients that dominate the signal at surface stations but occupy only a small fraction of a model grid cell. This dichotomy thus provides evidence supporting the important role of site representation error in the underestimation of modeled surface CO concentrations.

Aside from the overall positive bias of modeled CO column concentrations relative to satellite observations, the simulation-observation discrepancies exhibit noticeable regional variations: In China's highly industrialized NCP, modeled CO column concentrations show a negative bias of -16.6 ppb compared to satellite observations (Table S2.2); Similarly, the bias declines from continental averages to near-zero values in the Northeast US (3.1 to -0.6 ppb) and Central Europe (1.8 to 0.4 ppb) (Tables S3.2, S4.2). That is, in regions where local anthropogenic emissions exert strong control on surface and column CO concentrations (e.g., the NCP domain in China), the column bias tends to converge toward the surface bias. Conversely, in most other regions, the column comparison appears to be more influenced by large-scale signals (Figs. 1g-i).

3.2 Impacts of assimilations on atmospheric CO concentrations

3.2.1 Cross-validation of satellite and surface data assimilation

The preceding analysis suggests that the discrepancy between surface and column CO stems from a structural mismatch between point-like surface measurements and grid-scale satellite retrievals. To test this hypothesis directly, we now perform separate assimilation experiments using surface and satellite observations, and cross-validate their impacts on the resulting CO fields. As we expected, assimilation of MOPITT CO column data significantly improved the consistency between simulations and MOPIT observations: the a posteriori bias is close to zero in most regions, with slight positive biases remaining in a few remote areas, such as the Tibetan Plateau and low-latitude ocean areas (Figs. 5g-i). Scatter statistics also

https://doi.org/10.5194/egusphere-2026-4938
Preprint. Discussion started: 27 August 2026

indicate a marked improvement in consistency (Fig. 4): the *R* value increased from 0.22-0.73 to 0.72-0.87, and bias decreased from 1.8-6.8 ppb to 1.0-3.9 ppb across the three continents (Table 1.5). The *R* value showed even more substantial increases in various subregions: in the highly industrialized NCP, it rose from 0.11 to 0.71 (Table S2.5); in the Northeast US and Middle US, it increased from negative 0.06-0.02 to positive 0.67-0.75 (Table S3.5). Compared to assimilating satellite data, assimilating surface observation data brings a greater improvement in the agreement between the analysis field and surface observations (Figs. 5a-c). The *R* value increased from 0.23-0.31 to 0.94-0.95, and bias decreased from negative 331.4-198.9 ppb to negative 80.1-60.7 ppb across the three continents (Table 1.3).

However, an analysis field closer to surface observations does not necessarily imply better agreement with satellite observations. Cross-validation reveals that surface-based station assimilation introduces positive biases relative to MOPITT data (Figs. 5d-f). Compared to MOPITT satellite observations (sampled at locations of surface stations), assimilating surface observations causes the bias of modeled CO column concentrations to increase from 1.8-6.8 ppb to 5.4-27.1 ppb across three continents (Table 1.4). This result is consistent with the important role of site representation error in the difference between modeled and observed surface CO concentrations: the assimilations add positive CO increments to surface layer to reduce negative bias at surface level, and these positive CO increments are transported vertically into the free troposphere, ultimately leading to an overall positive bias relative to satellite column observations.

3.2.2 Regional mechanisms behind surface assimilation impacts on CO columns

The impact of surface observation assimilation on CO columns exhibits noticeable regional differences: in China and Europe, assimilating surface observations leads to a significant increase in the bias relative to satellite observations (Table 1.4), from 6.8 ppb to 27.1 ppb (China) and from 1.8 ppb to 10.5 ppb (Europe). However, in North America,

https://doi.org/10.5194/egusphere-2026-4938
Preprint. Discussion started: 27 August 2026

assimilating surface observations results in only a slight increase in the bias, from 3.1 ppb to 5.4 ppb. Why is there such a difference between North America and China/Europe? To understand the source of this discrepancy, Fig. 6 illustrates the impact of surface observation assimilation on atmospheric CO concentrations at different altitudes. In China and Europe, surface observation assimilation results in widespread and significant enhancements in surface CO concentrations (Figs. 6a, 6k), whereas in North America, both the magnitude and spatial extent of these enhancements are notably smaller (Fig. 6f). This weaker surface enhancement in North America can be attributed to two interrelated factors. First, the model's systematic underestimation of surface CO is less severe in North America than in China or Europe (Fig. 2), reducing the magnitude of positive increments needed. Second, the sparser surface observation network in North America (430 stations vs. 1931 in China and 984 in Europe) further limits the total positive CO increments introduced by assimilation.

The weaker column impact over North America arises from additional factors beyond those controlling surface increments. As noted by Jiang et al. (2015), the vertical transport of surface CO into the free troposphere occurs slower in North America than in East Asia, suppressing the upward propagation of these increments. Furthermore, transboundary transport further modulates the regional imprint of surface assimilation. North America and China lie on similar latitudinal bands, meaning that the free tropospheric CO over North America is strongly influenced by the Asian outflow, a dominant global source of CO. In this context, locally emitted CO from North American surface sources competes with a strong imported background, diluting the vertical propagation signal of positive increments added by surface assimilation. Conversely, European surface CO competes primarily with the North American outflow, where the two source strengths are more comparable. Therefore, in Europe, the additional CO from surface assimilation is less diluted by the background flow, allowing a more effective upward propagation. The combined effect of these factors is that the impact of positive CO increments

https://doi.org/10.5194/egusphere-2026-4938
Preprint. Discussion started: 27 August 2026

resulting from surface observation assimilation can effectively propagate upward to the 400 hPa level in East Asia (Fig. 6d) and to the 600 hPa level in Europe (Fig. 6m), but are largely confined to the lower troposphere in North America (Figs. 6f-g).

3.3 Decadal trends in CO concentrations in observations and assimilations

Given the structural divergence revealed by the assimilation experiments, we next examine whether this divergence also manifests in the decadal trends of CO concentrations. Surface observations indicate a significant decreasing trend in CO concentrations: in China, surface CO concentration decreased at a rate of -43.6 ppb yr^{-1} (-5.92% yr^{-1}) (Table 3), with the highly polluted NCP showing a stronger decline of -68.3 ppb yr^{-1} (-8.25% yr^{-1}) (Table S5). In contrast, weaker trends were observed in North America and Europe: -5.3 ppb yr^{-1} (-1.51% yr^{-1}) in North America and -3.9 ppb yr^{-1} (-1.02% yr^{-1}) in Europe. Beyond the overall downward trends, distinct interannual variations in CO concentrations exist across the three regions (Fig. 7). Surface CO concentrations in China have generally exhibited a sustained decline. Correspondingly, the declining trends in North America and Europe are largely driven by earlier reductions in CO concentrations: in North America, the overall downward trend in surface CO concentrations leveled off after 2018 (Fig. 7e); in Europe, it plateaued after 2016 (Fig. 7i). The interannual evolution of surface CO concentrations broadly aligns with recent CO emission estimates derived from MOPITT CO retrievals: Tang et al. (2026) reported that anthropogenic CO emissions in China continuously decreased between 2015 and 2022, while the declining trends in anthropogenic CO emissions in the US and Europe have stalled in recent years.

The Kalman filter assimilation based on surface CO observations effectively captures the observed decreasing trends: the declining trends in assimilated surface CO fields are -5.38% yr^{-1}, -1.36% yr^{-1}, and -1.18% yr^{-1} for China, North America, and Europe, respectively. As shown in Figures 8a-c, assimilated surface CO concentrations exhibit an overall decline across

https://doi.org/10.5194/egusphere-2026-4938
Preprint. Discussion started: 27 August 2026

China; correspondingly, more pronounced regional differences appear in North America and Europe: scattered hotspots of increasing CO concentrations are found in the south-central US, while Europe displays more country-level variability: regions with rising CO concentrations are clustered in the Iberian Peninsula, Slovakia, Hungary, Serbia, and Turkey, with sporadic occurrences in Czechia and the Apennine Peninsula.

MOPITT observations also show a decreasing trend in CO column concentrations from 2015 to 2024, but the rate of decrease is significantly lower than that of surface observations. In China, the CO column concentration decreases at a rate of -0.79 ± 0.40 ppb yr^{-1} (-0.77% yr^{-1}) (Table 3), with the highly polluted NCP reaching a trend of -2.65 ± 0.64 ppb yr^{-1} (-1.85% yr^{-1}) (Table S5). North America and Europe show only insignificant decreasing trends: -0.11 ± 0.70 ppb yr^{-1} (-0.11% yr^{-1}) in North America and -0.21 ± 0.65 ppb yr^{-1} (-0.21% yr^{-1}) in Europe. Furthermore, CO column concentrations in North America and Europe exhibit substantial interannual variability during 2020-2024 (Fig. 9), with notably low values occurring in 2022. As shown in Fig. S1, compared to 2021, CO column concentrations at high northern latitudes in 2022 were significantly lower, and the extreme low-value areas occurred over high-latitude North America and eastern Siberia, which overlap with high-latitude boreal fire regions (Zheng et al., 2023; Tang et al., 2026). Therefore, the interannual variability of CO column concentrations during 2020-2024 reflects the influence of wildfire emissions.

The Kalman filter assimilation (KF-MOPITT) captures the decreasing trend in CO column concentrations reasonably well: the assimilated CO column concentration trends are -0.50% yr^{-1}, -0.11% yr^{-1}, and -0.10% yr^{-1} for China, North America, and Europe, respectively. As shown in Figs. 8g-i, the assimilated CO column concentration field still shows an overall decreasing trend in China, but the declining trends are markedly reduced in the US and Europe. Correspondingly, the a posteriori CO column concentrations derived from KF-Surface exhibit a significantly higher decreasing trend in China (-0.97% yr^{-1}) than that from satellite

https://doi.org/10.5194/egusphere-2026-4938
Preprint. Discussion started: 27 August 2026

assimilation. Although the a posteriori CO column concentration trends in North America and Europe are numerically similar to those from KF-MOPITT, i.e., -0.15% yr^{-1} (US) and -0.14% yr^{-1} (Europe) in KF-Surface, their spatial distributions (Figs. 8d-f) differ markedly from KF-MOPITT: they show a more pronounced decreasing trend in China (Fig. 8d) and also exhibit overall decreasing trends in North America and Europe (Figs. 8e-f). This suggests that the assimilation results from KF-Surface reflect more strongly the influence of local CO emissions. This is also reflected in their interannual evolution: as shown in Fig. 9, the a posteriori CO column concentrations generated by KF-Surface remain roughly stable during 2020-2024, unaffected by high-latitude wildfire emissions.

4. Conclusion

This study presents a comprehensive multi-region analysis of atmospheric CO over China, North America, and Europe from 2015 to 2024, leveraging both MOPITT satellite retrievals and ground-based observations. Our results confirm that the model's systematic underestimation of surface CO concentrations is a common feature across all three regions. The median observation-to-model ratio is 1.82 in China, 1.65 in North America, and 2.25 in Europe, indicating a widespread negative bias in modeled surface CO. This bias diminishes progressively from urban to rural sites, by 44% in North America and 58% in Europe, and almost disappears at remote sites, suggesting that representation error is an important driver of the surface-model discrepancy. In contrast, comparisons of column CO between MOPITT and the model reveal no systematic underestimation; biases are slightly positive across all continents (1.8-6.8 ppb).

Assimilation experiments illuminate the nature of this divergence. While surface-data assimilation greatly improves agreement with in situ observations ($R > 0.94$), it introduces a positive bias in column CO relative to MOPITT, especially over China (27.1 ppb) and Europe

https://doi.org/10.5194/egusphere-2026-4938
Preprint. Discussion started: 27 August 2026

(10.5 ppb). In North America, however, surface assimilation increases the column bias slightly to 5.4 ppb, owing to a combination of weaker model bias, sparser observational networks, slower vertical transport, and dilution by strong transboundary inflow from Asia. These regional differences underscore that the satellite-surface discrepancy is a structurally embedded feature of the observing system, modulated by local meteorology, network density, and background transport. Consistent with this structural divergence, decadal trend analyses show that surface CO concentrations declined sharply in China (-5.92% yr^{-1}), while trends in North America and Europe were plateaued after 2018 and 2016, respectively. Satellite-derived column trends were substantially weaker, particularly in North America and Europe, where recent interannual variability was dominated by boreal wildfire emissions. Thus, assimilated fields from surface observations captured local emission-driven trends, while satellite-based assimilations reflected broader, transport-influenced signals.

Taken together, our multi-region analysis clarifies the complementary roles of surface and satellite CO observations. Surface measurements capture local emission signals and their temporal trends with high fidelity, yet their quantitative use for emission strength estimation is hampered by unresolved representation errors. Satellite retrievals, while insensitive to such representativity issues, exhibit dampened temporal trends due to the influence of broad-scale background transport. These intrinsic differences imply that neither observation type alone may not be able to fully characterize CO emissions. We therefore advocate for future inversion studies to jointly utilize both observation platforms, systematically comparing and reconciling the emission estimates derived from surface and satellite data. Such a synergistic framework will enable a more robust and self-consistent assessment of CO emissions, leveraging the strengths of each observation type while mitigating their respective limitations.

Data availability: The MEE data can be downloaded from https://quotsoft.net/air/. The AQS

https://doi.org/10.5194/egusphere-2026-4938
Preprint. Discussion started: 27 August 2026

data can be downloaded from https://aqs.epa.gov/aqsweb/airdata/download_files.html. The NAPS data can be downloaded from https://data-donnees.az.ec.gc.ca/data/air/monitor/national-air-pollution-surveillance-naps-program?lang=en. The EEA data can be downloaded from https://eeadmz1-downloads-webapp.azurewebsites.net/. The MOPITT data can be downloaded from https://asdc.larc.nasa.gov/data/MOPITT/. The GEOS-Chem model (version 14.6.2) can be downloaded from https://github.com/geoschem/geos-chem/releases#release-14.6.2.

Author Contributions: Z.J. designed the research. Z.T. performed the research. Z.J. and Z.T. wrote the manuscript. All authors contributed to discussions and editing the manuscript.

Competing interests: The authors declare that they have no conflict of interest.

Acknowledgments: We thank the providers of the MOPITT CO data. We thank the Ministry of Ecology and Environment of China for providing the MEE surface measurements; US Environmental Protection Agency for providing the AQS surface observations; the Environment and Climate Change Canada for providing the NAPS data, and the European Environment Agency for providing the EEA data. This work was supported by the National Natural Science Foundation of China (42277082).

References

Castellanos, P., Marufu, L. T., Doddridge, B. G., Taubman, B. F., Schwab, J. J., Hains, J. C., Ehrman, S. H., and Dickerson, R. R.: Ozone, oxides of nitrogen, and carbon monoxide during pollution events over the eastern United States: An evaluation of emissions and vertical mixing, J. Geophys. Res.-Atmos., 116, D16307, 10.1029/2010jd014540, 2011.

Deeter, M., Francis, G., Gille, J., Mao, D., Martínez-Alonso, S., Worden, H., Ziskin, D., Drummond, J., Commane, R., Diskin, G., and McKain, K.: The MOPITT Version 9 CO

https://doi.org/10.5194/egusphere-2026-4938
Preprint. Discussion started: 27 August 2026

product: sampling enhancements and validation, Atmos. Meas. Tech., 15, 2325-2344, 10.5194/amt-15-2325-2022, 2022.

Du, Q., Zhao, C., Zhang, M., Dong, X., Chen, Y., Liu, Z., Hu, Z., Zhang, Q., Li, Y., Yuan, R., and Miao, S.: Modeling diurnal variation of surface $PM_{2.5}$ concentrations over East China with WRF-Chem: impacts from boundary-layer mixing and anthropogenic emission, Atmos. Chem. Phys., 20, 2839-2863, 10.5194/acp-20-2839-2020, 2020.

Elbern, H., Strunk, A., Schmidt, H., and Talagrand, O.: Emission rate and chemical state estimation by 4-dimensional variational inversion, Atmos. Chem. Phys., 7, 3749-3769, 10.5194/acp-7-3749-2007, 2007.

Fang, C., Jiang, Z., Wang, M., Chen, X., Han, W., He, T.-L., and Shen, Y.: Quantifying and correcting systematic discrepancies in the comparison between surface CO observations and simulations, Atmos. Environ., 368, 121769, 10.1016/j.atmosenv.2025.121769, 2026.

Fang, L., Jin, J., Segers, A., Li, K., Xia, J., Han, W., Li, B., Lin, H. X., Zhu, L., Liu, S., and Liao, H.: Observational operator for fair model evaluation with ground NO_2 measurements, Geosci. Model Dev., 17, 8267-8282, 10.5194/gmd-17-8267-2024, 2024.

Feng, S., Jiang, F., Wang, H., Wang, H., Ju, W., Shen, Y., Zheng, Y., Wu, Z., and Ding, A.: NO_x Emission Changes Over China During the COVID-19 Epidemic Inferred From Surface NO_2 Observations, Geophys. Res. Lett., 47, e2020GL090080, 10.1029/2020GL090080, 2020a.

Feng, S., Jiang, F., Wu, Z., Wang, H., Ju, W., and Wang, H.: CO Emissions Inferred From Surface CO Observations Over China in December 2013 and 2017, J. Geophys. Res.-Atmos., 125, e2019JD031808, 10.1029/2019jd031808, 2020b.

Fortems-Cheiney, A., Broquet, G., Potier, E., Plauchu, R., Berchet, A., Pison, I., Denier van der Gon, H., and Dellaert, S.: CO anthropogenic emissions in Europe from 2011 to 2021: insights from Measurement of Pollution in the Troposphere (MOPITT) satellite data, Atmos. Chem. Phys., 24, 4635-4649, 10.5194/acp-24-4635-2024, 2024.

Guenther, A., Karl, T., Harley, P., Wiedinmyer, C., Palmer, P. I., and Geron, C.: Estimates of global terrestrial isoprene emissions using MEGAN (Model of Emissions of Gases and Aerosols from Nature), Atmos. Chem. Phys., 6, 3181-3210, 10.5194/acp-6-3181-2006, 2006.

Han, H., Liu, J., Yuan, H., Jiang, F., Zhu, Y., Wu, Y., Wang, T., and Zhuang, B.: Impacts of Synoptic Weather Patterns and their Persistency on Free Tropospheric Carbon Monoxide Concentrations and Outflow in Eastern China, J. Geophys. Res.-Atmos., 123, 7024-7046, 10.1029/2017jd028172, 2018.

Han, W., He, T.-L., Tang, Z., Wang, M., Jones, D., and Jiang, Z.: A comparative analysis for a deep learning model (hyDL-CO v1.0) and Kalman filter to predict CO concentrations in China, Geosci. Model Dev., 15, 4225-4237, 10.5194/gmd-15-4225-2022, 2022.

Hoesly, R. M., Smith, S. J., Feng, L., Klimont, Z., Janssens-Maenhout, G., Pitkanen, T., Seibert, J. J., Vu, L., Andres, R. J., Bolt, R. M., Bond, T. C., Dawidowski, L., Kholod, N., Kurokawa, J. I., Li, M., Liu, L., Lu, Z., Moura, M. C. P., O'Rourke, P. R., and Zhang, Q.: Historical (1750–2014) anthropogenic emissions of reactive gases and aerosols from the Community Emissions Data System (CEDS), Geosci. Model Dev., 11, 369-408, 10.5194/gmd-11-369-2018, 2018.

https://doi.org/10.5194/egusphere-2026-4938
Preprint. Discussion started: 27 August 2026

Jeffery, P. S., Drummond, J. R., Zou, J., and Walker, K. A.: Identifying episodic carbon monoxide emission events in the MOPITT measurement dataset, Atmos. Chem. Phys., 24, 4253-4263, 10.5194/acp-24-4253-2024, 2024.

Jia, M., Jiang, F., Evangeliou, N., Eckhardt, S., Stohl, A., Huang, X., Shen, Y., Feng, S., He, W., Wang, J., Wang, H., Wu, M., Ju, W., and Ding, A.: Anthropogenic Carbon Monoxide Emissions During 2014–2020 in China Constrained by In Situ Ground Observations, J. Geophys. Res.-Atmos., 130, e2024JD042371, 10.1029/2024jd042371, 2025.

Jiang, Z., Jones, D. B. A., Worden, H. M., Deeter, M. N., Henze, D. K., Worden, J., Bowman, K. W., Brenninkmeijer, C. A. M., and Schuck, T. J.: Impact of model errors in convective transport on CO source estimates inferred from MOPITT CO retrievals, J. Geophys. Res.-Atmos., 118, 2073-2083, 10.1002/jgrd.50216, 2013.

Jiang, Z., Jones, D. B. A., Worden, H. M., and Henze, D. K.: Sensitivity of top-down CO source estimates to the modeled vertical structure in atmospheric CO, Atmos. Chem. Phys., 15, 1521-1537, 10.5194/acp-15-1521-2015, 2015.

Li, M., Kurokawa, J., Zhang, Q., Woo, J. H., Morikawa, T., Chatani, S., Lu, Z., Song, Y., Geng, G., Hu, H., Kim, J., Cooper, O. R., and McDonald, B. C.: MIXv2: a long-term mosaic emission inventory for Asia (2010–2017), Atmos. Chem. Phys., 24, 3925-3952, 10.5194/acp-24-3925-2024, 2024.

Miyazaki, K., Eskes, H., Sudo, K., Boersma, K. F., Bowman, K., and Kanaya, Y.: Decadal changes in global surface NOx emissions from multi-constituent satellite data assimilation, Atmos. Chem. Phys., 17, 807-837, 10.5194/acp-17-807-2017, 2017.

Tang, W., Gaubert, B., Emmons, L., Ziskin, D., Mao, D., Edwards, D., Arellano, A., Raeder, K., Anderson, J., and Worden, H.: Advantages of assimilating multispectral satellite retrievals of atmospheric composition: a demonstration using MOPITT carbon monoxide products, Atmos. Meas. Tech., 17, 1941-1963, 10.5194/amt-17-1941-2024, 2024.

Tang, Z., Chen, J., and Jiang, Z.: Discrepancy in assimilated atmospheric CO over East Asia in 2015–2020 by assimilating satellite and surface CO measurements, Atmos. Chem. Phys., 22, 7815-7826, 10.5194/acp-22-7815-2022, 2022.

Tang, Z., Yang, P., Miyazaki, K., Worden, J., Worden, H., Henze, D. K., Jones, D. B. A., and Jiang, Z.: Global CO emissions and drivers of atmospheric CO trends constrained by MOPITT satellite measurements, Atmos. Chem. Phys., 26, 5531-5551, 10.5194/acp-26-5531-2026, 2026.

van der Werf, G. R., Randerson, J. T., van Wees, D., Chen, Y., Giglio, L., Hall, J., Vernooij, R., Mu, M., Binte Shahid, S., Barsanti, K. C., Yokelson, R., and Morton, D. C.: Landscape fire emissions from the 5th version of the Global Fire Emissions Database (GFED5), Scientific Data, 12, 1870, 10.1038/s41597-025-06127-w, 2025.

Wei, J., Li, Z., Wang, J., Li, C., Gupta, P., and Cribb, M.: Ground-level gaseous pollutants (NO_2, SO_2, and CO) in China: daily seamless mapping and spatiotemporal variations, Atmos. Chem. Phys., 23, 1511-1532, 10.5194/acp-23-1511-2023, 2023.

Worden, H. M., Deeter, M. N., Edwards, D. P., Gille, J. C., Drummond, J. R., and Nédélec, P.: Observations of near-surface carbon monoxide from space using MOPITT multispectral retrievals, J. Geophys. Res.-Atmos., 115, D18314, 10.1029/2010jd014242, 2010.

https://doi.org/10.5194/egusphere-2026-4938
Preprint. Discussion started: 27 August 2026

568 Xie, Y., Han, H., and Liu, J.: Spatial and seasonal variations and trends in carbon monoxide
569 over China during 2013–2022, Atmos. Environ., 350, 121163,
570 10.1016/j.atmosenv.2025.121163, 2025.
571 Zheng, B., Chevallier, F., Yin, Y., Ciais, P., Fortems-Cheiney, A., Deeter, M. N., Parker, R. J.,
572 Wang, Y., Worden, H. M., and Zhao, Y.: Global atmospheric carbon monoxide budget 2000–
573 2017 inferred from multi-species atmospheric inversions, Earth Syst. Sci. Data, 11, 1411-
574 1436, 10.5194/essd-11-1411-2019, 2019.
575 Zheng, B., Ciais, P., Chevallier, F., Yang, H., Canadell, J. G., Chen, Y., van der Velde, I. R.,
576 Aben, I., Chuvieco, E., Davis, S. J., Deeter, M., Hong, C., Kong, Y., Li, H., Li, H., Lin, X.,
577 He, K., and Zhang, Q.: Record-high CO_2 emissions from boreal fires in 2021, Science, 379,
578 912-917, 10.1126/science.ade0805, 2023.
579 Zhou, Y., Mao, H., Demerjian, K., Hogrefe, C., and Liu, J.: Regional and Hemispheric
580 Influences on Temporal Variability in Baseline Carbon Monoxide and Ozone over the
581 Northeast US, Atmos Environ (1994), 164, 309-324, 10.1016/j.atmosenv.2017.06.017, 2017.
582

https://doi.org/10.5194/egusphere-2026-4938
Preprint. Discussion started: 27 August 2026

Experiments		Dataset for evaluation	Domain	R	Slope	Bias (ppb)	RMSE (ppb)
T1.1	a priori simulation	Surface	China	0.31	0.22	-331.4	512.8
			North America	0.23	0.07	-198.9	282.2
			Europe	0.29	0.03	-244.7	378.7
T1.2	a priori simulation	MOPITT	China	0.73	0.62	6.8	18.8
			North America	0.30	0.14	3.1	13.7
			Europe	0.22	0.08	1.8	11.4
T1.3	KF-Surface	Surface	China	0.94	0.80	-80.1	157.0
			North America	0.95	0.72	-68.8	102.3
			Europe	0.95	0.71	-60.7	128.9
T1.4	KF-Surface	MOPITT (sampled)	China	0.76	0.98	27.1	33.9
			North America	0.44	0.27	5.4	14.8
			Europe	0.46	0.33	10.5	14.9
T1.5	KF-MOPITT	MOPITT	China	0.87	0.74	3.9	13.0
			North America	0.80	0.55	1.6	8.6
			Europe	0.72	0.45	1.0	8.0

Table. 1. Statistical metrics comparing simulations and assimilations against surface and MOPITT data across China, North America and Europe. Three different experiments are performed, namely the GEOS-Chem a priori simulation (T1.1, T1.2), the Kalman Filter assimilation of surface CO observations (T1.3, T1.4), and the Kalman Filter assimilation of MOPITT CO column observations (T1.5). The evaluation employs three distinct datasets: surface measurements, MOPITT retrievals and a sampled MOPITT dataset matching locations of surface stations. Please check Tables S2-S4 for the statistical information of each subregion.

Domain	Variable	All sites	Urban	Suburban	Rural	Remote
China	Number of sites	1931	1703	228	/	/
	Obs/Mod (mean)	2.08	2.05	2.27	/	/
	Obs/Mod (median)	1.82	1.80	1.96	/	/
North Ameirca	Number of sites	430	228	130	52	20
	Obs/Mod (mean)	1.92	1.98	2.03	1.62	1.26
	Obs/Mod (median)	1.65	1.77	1.64	1.43	1.21
Europe	Number of sites	984	742	159	70	3
	Obs/Mod (mean)	2.52	2.64	2.33	1.82	0.95
	Obs/Mod (median)	2.25	2.30	2.17	1.55	0.94

Table 2. Obs/Mod ratios of surface CO concentrations over China, North America and Europe in 2015-2024. Surface observation sites are categorized into five types: all sites, as well as urban (including both traffic and urban sites in this Table), suburban, rural and remote sites. Data for China are presented for urban and suburban sites only, as rural and remote data are unavailable.

https://doi.org/10.5194/egusphere-2026-4938
Preprint. Discussion started: 27 August 2026

Experiments		China		North America		Europe	
		Mean	Trend	Mean	Trend	Mean	Trend
Surface (ppb or ppb/year)	a priori simulation	401.3	-6.84 ± 5.27	172.1	-0.20 ± 1.42	140.3	-0.26 ± 0.33
	surface obs	735.3	-43.55 ± 7.51	349.4	-5.29 ± 3.12	385.0	-3.91 ± 4.01
	KF-surface	654.6	-35.21 ± 6.56	287.6	-3.91 ± 2.17	324.3	-3.82 ± 2.59
Column (Xco ppb or ppb/year)	a priori simulation	109.3	-0.28 ± 0.14	98.9	-0.10 ± 0.10	98.9	-0.02 ± 0.07
	MOPITT column	102.4	-0.79 ± 0.40	95.7	-0.11 ± 0.70	97.1	-0.21 ± 0.65
	KF-surface	120.9	-1.17 ± 0.18	100.2	-0.15 ± 0.13	103.6	-0.14 ± 0.13
	KF-MOPITT	106.4	-0.53 ± 0.24	97.4	-0.11 ± 0.42	98.1	-0.10 ± 0.32

Table 3. Averages and trends of surface and column CO concentrations from different experiments and datasets in 2015-2024.

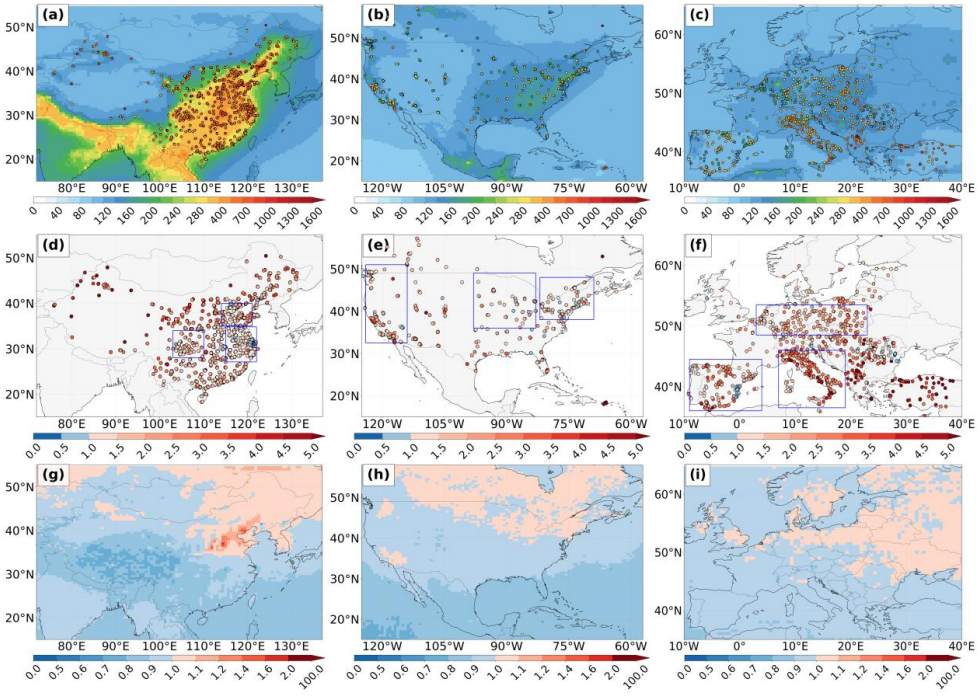

Fig. 1. (a-c) Modeled (contour, a priori simulation) and observed (dotted) surface CO concentrations in 2015-2024 with unit ppb; (d-f) Ratios between observed and modeled surface CO concentrations in 2015-2024. The blue boxes define the subregions of North China Plain (NCP), Yangtze River Delta (YRD), and Sichuan Basin (SCB) for China; Northeast, Middle and West Coast for North America; and Iberian Peninsula, Apennine Peninsula and Central Europe for Europe. (g-i) Ratios between MOPITT and modeled CO column concentrations in 2015-2024.

https://doi.org/10.5194/egusphere-2026-4938
Preprint. Discussion started: 27 August 2026

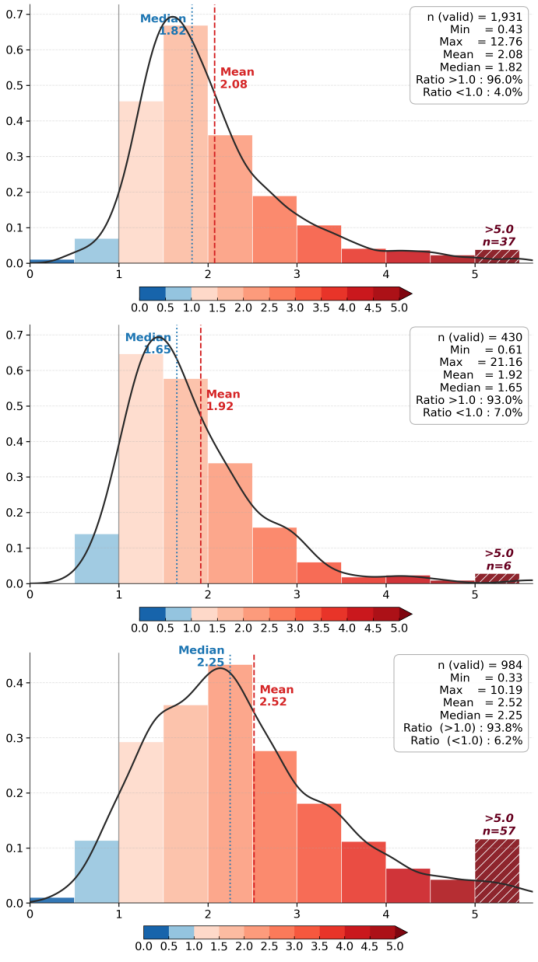

Fig. 2. Distribution of Obs/Mod ratios of surface CO concentrations over China, North America and Europe in 2015-2024. Please check the statistical metrics for different site types in Table 2.

https://doi.org/10.5194/egusphere-2026-4938
Preprint. Discussion started: 27 August 2026

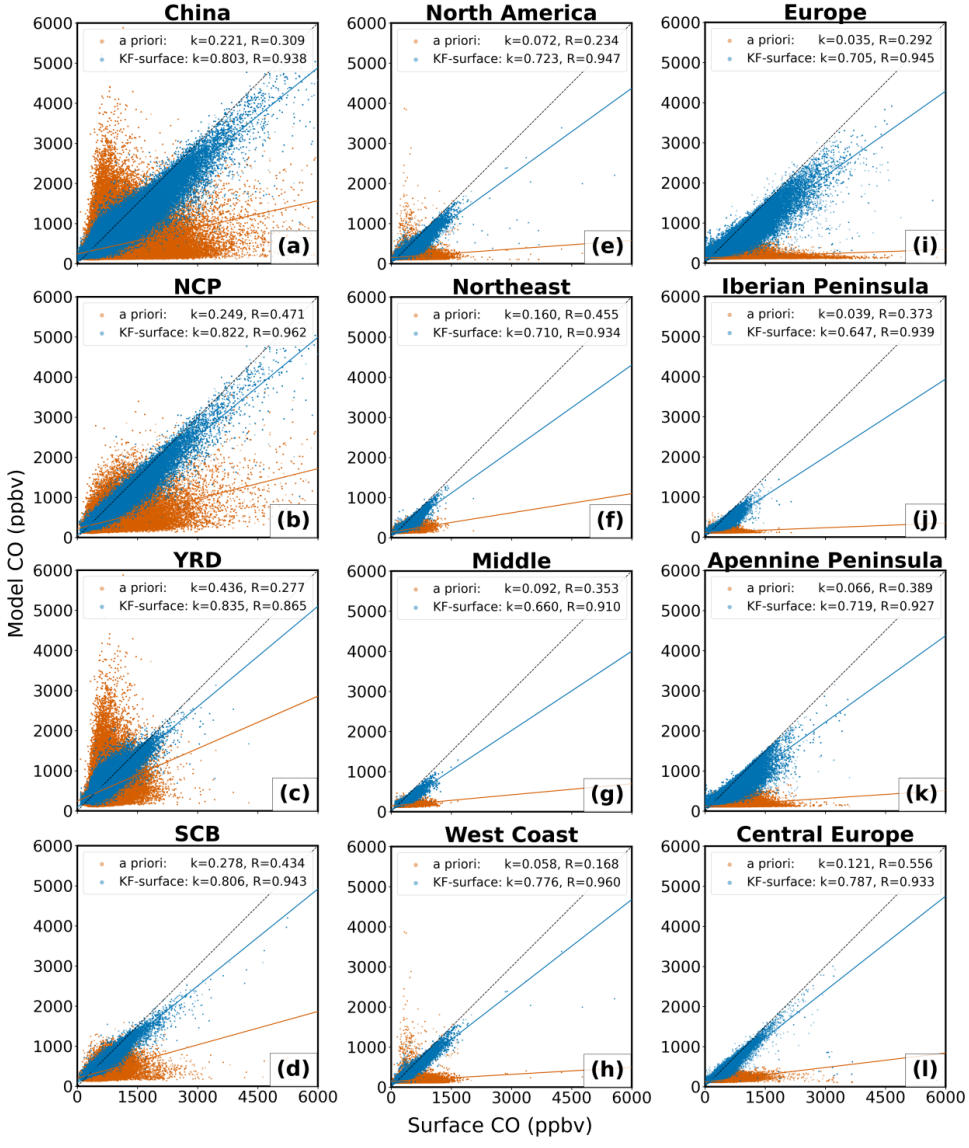

Fig. 3. Relationships of simulations (red) and assimilations (KF-Surface, blue) against surface CO observations across China, North America, and Europe, along with their respective subregions in 2015-2024.

https://doi.org/10.5194/egusphere-2026-4938
Preprint. Discussion started: 27 August 2026

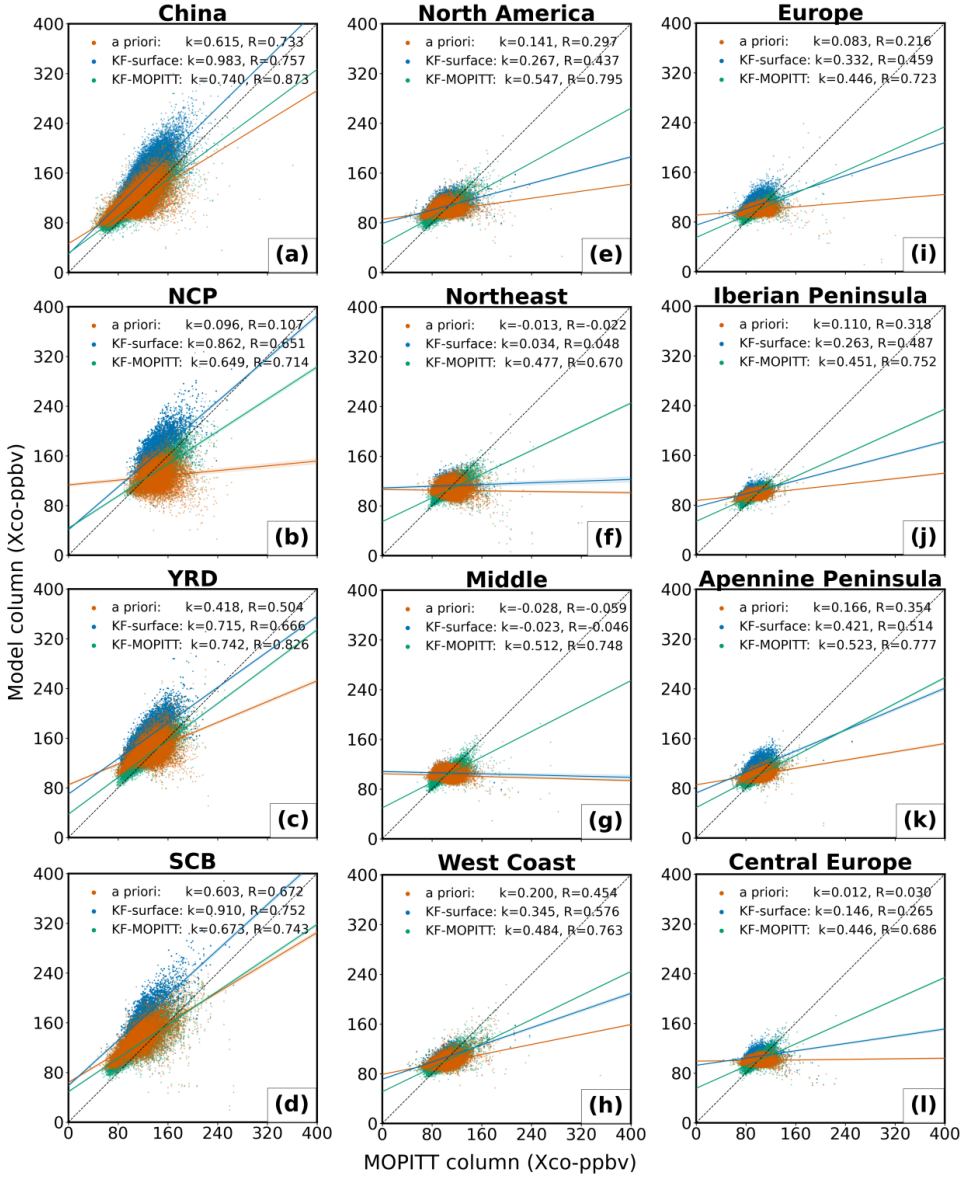

Fig. 4. Relationships of simulations (red) and assimilations against MOPITT CO observations across China, North America, and Europe, along with their respective subregions in 2015-2024. The assimilation here includes the KF-MOPITT (green) and KF-Surface (blue). Note sampled MOPITT dataset matching the locations of surface stations is compared with KF-Surface.

https://doi.org/10.5194/egusphere-2026-4938
Preprint. Discussion started: 27 August 2026

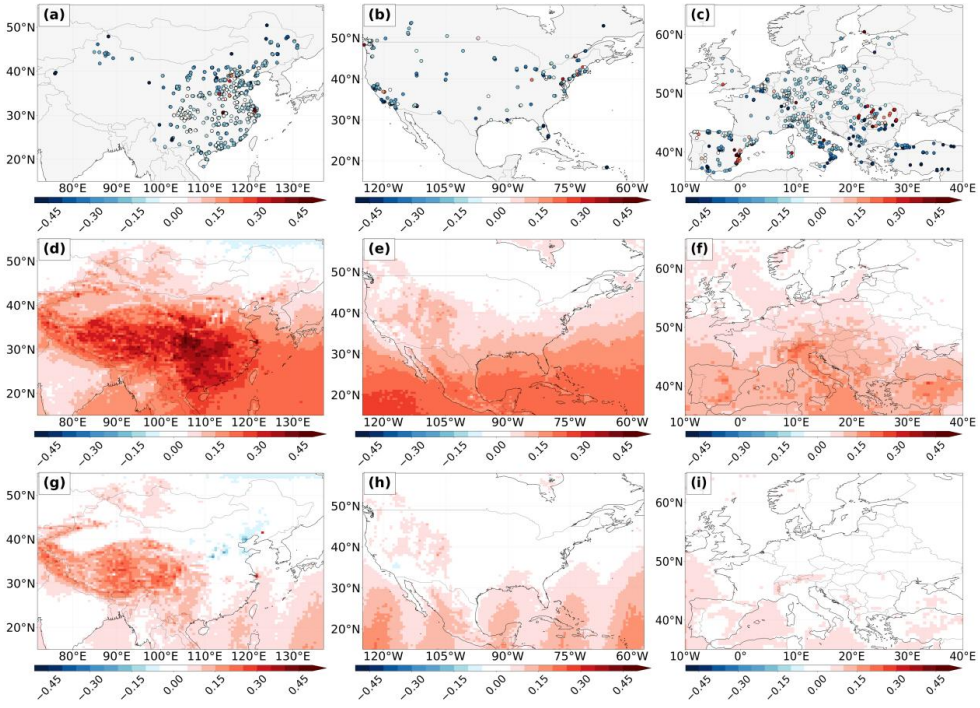

Fig. 5. (a-c) Relative difference of CO concentrations from KF-Surface to surface observations. (d-f) Relative difference of CO concentrations from KF-Surface to MOPITT observations. (g-i) Relative difference of CO concentrations from KF-MOPITT to MOPITT observations. The calculation method for relative difference is (model − observation) / observation.

https://doi.org/10.5194/egusphere-2026-4938
Preprint. Discussion started: 27 August 2026

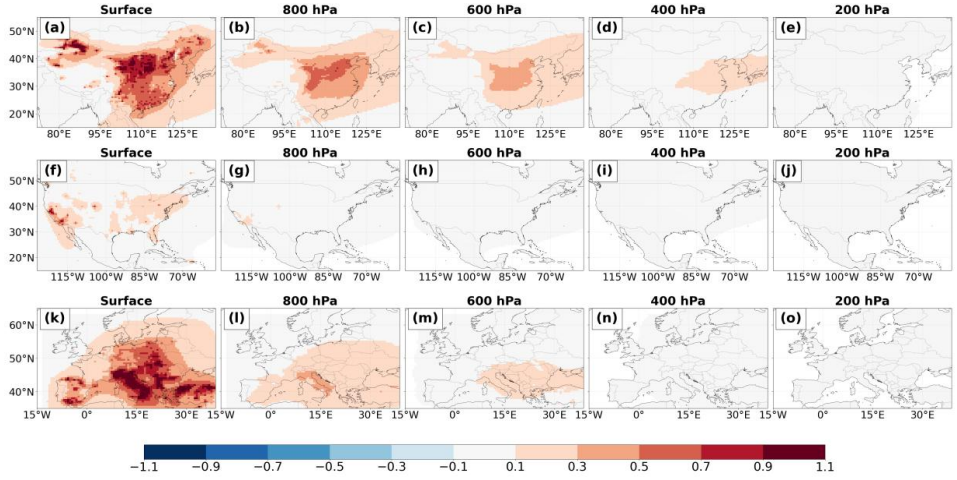

Fig. 6. Relative difference of CO concentrations from KF-Surface to the GEOS-Chem a priori simulation at different vertical levels over (a–e) East Asia, (f–j) North America, and (k–o) Europe. From left to right, the results are shown at the surface, 800 hPa, 600 hPa, 400 hPa, and 200 hPa, respectively. The calculation method for relative difference is (a posteriori - a priori) / a priori.

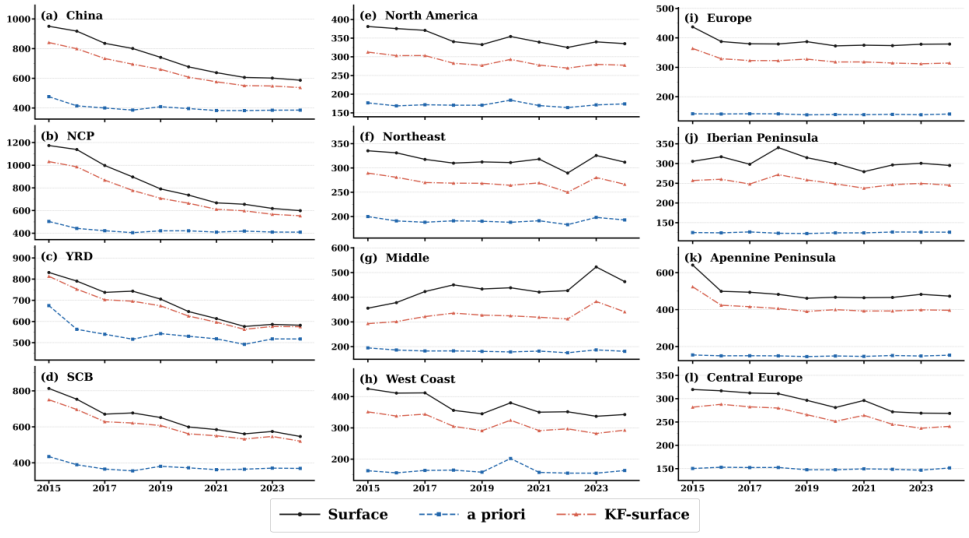

Fig. 7. Surface CO concentrations from surface observations (black), GEOS-Chem a priori simulations (blue) and assimilations of KF-Surface (red).

https://doi.org/10.5194/egusphere-2026-4938
Preprint. Discussion started: 27 August 2026

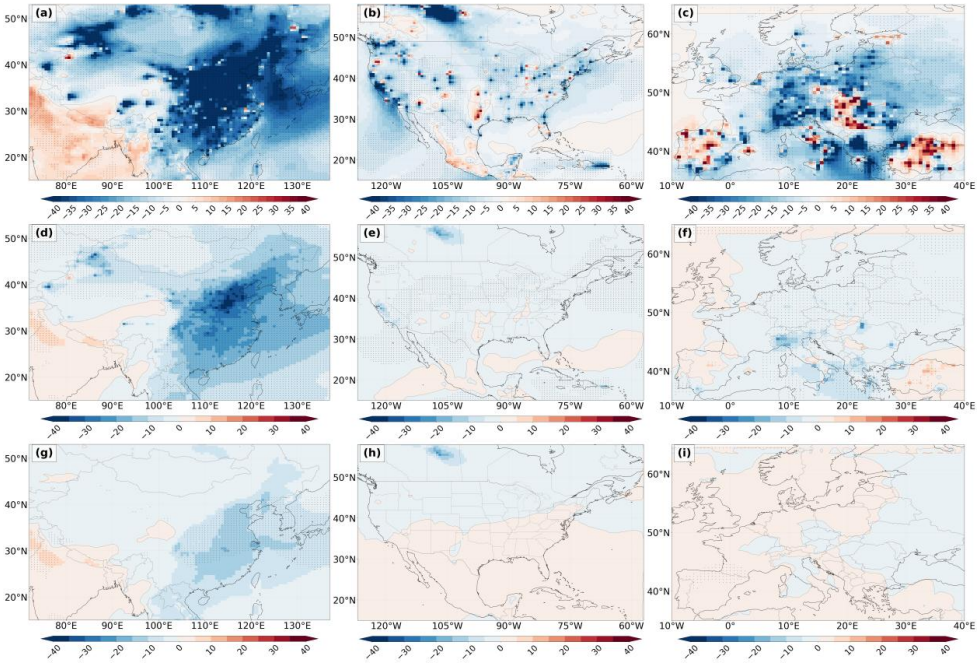

Fig. 8. Trends of surface CO concentrations from KF-Surface (a-c), as well as trends of CO columns from KF-Surface (d-f) and KF-MOPITT (g-i) in 2015-2024.

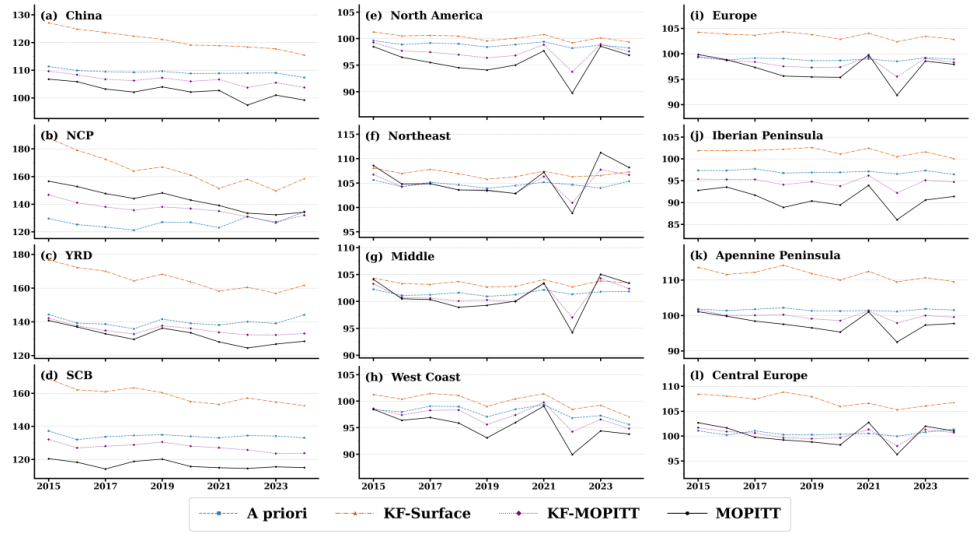

Fig. 9. CO columns from MOPITT observations (black), GEOS-Chem a priori simulations (blue) as well as assimilations of KF-Surface (red) and KF-MOPITT (magenta).